ACS APPLIED NANO MATERIALS
Cite This: ACS Appl. Nano Mater. 2018, 1, 1819−1827
Article
www.acsanm.org

Multifunctional Metallo-Organic Vesicles Displaying Aggregation-Induced Emission: Two-Photon Cell-Imaging, Drug Delivery, and Specific Detection of Zinc Ion

Ying Wei,[†] Lizhi Wang,[‡] Jianbin Huang,[†] Junfang Zhao,[‖] and Yun Yan*[,†]

[†]Beijing National Laboratory for Molecular Sciences (BNLMS), State Key Laboratory for Structural Chemistry of Unstable and Stable Species, College of Chemistry and Molecular Engineering, Peking University, Beijing 100871, P. R. China

[‡]College of Chemistry and Chemical Engineering, Xinjiang University, Urumqi 830046, P. R. China

[‖]Technical Institute of Physics and Chemistry, Chinese Academy of Sciences, Beijing 100871, China

Supporting Information

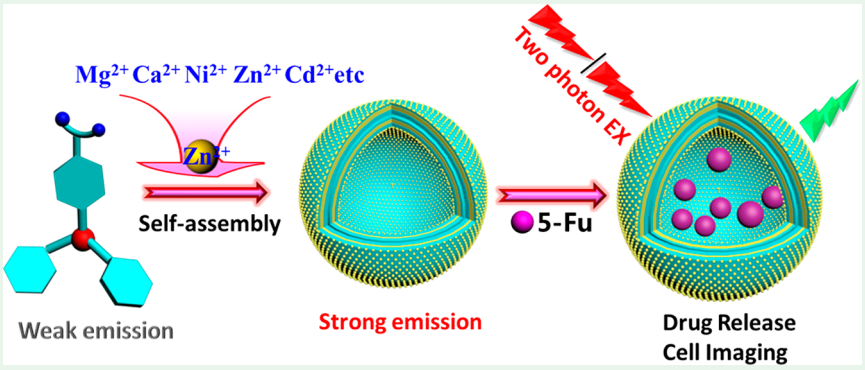

ABSTRACT: Molecules displaying aggregation-induced emission (AIE) property can hardly self-assemble into vesicles desired in design of theranostics. We report the formation of metallo-organic AIE vesicles with triarylamine carboxylate (TPA-1) and Zn^{2+} ions. TPA-1 shows a great binding affinity to Zn^{2+} as a fluorescence turn-on sensor. The vesicles exhibited high fluorescence-emission property under two-photon mode which endows them very good cell imaging ability. Drug-loading experiments suggest a loading capacity for the model anticancer drug 5-fluorouracil (5-Fu) can reach up to 53.4%, and sustained release of the drug is possible in biological environment. This is the first report of supramolecular coordination fluorescent vesicles based on AIE molecule. Further study reveals the fluorescence enhancement of TPA-1 can only be triggered by Zn^{2+}, suggesting the ability of specific detection of Zn^{2+}. This study indicates that the formation of metallo-organic vesicles can be a multiplatform for cell-imaging, drug carrier, and metal ions detection.

KEYWORDS: *aggregation-induced emission, fluorescence, metallo-organic vesicles, zinc ion, two-photon, drug release*

1. INTRODUCTION

The last decade has witnessed the rapid development of aggregation-induced emission (AIE).[1−3] Molecules displaying AIE ability are usually nonplannar, where intromolecular motion results in nonradiating energy decay. For this reason, these molecules are non or weakly emissive in solution, but become highly luminescent in the condensed state because of the suppression of the intramolecualr motions.[1] This unique AIE property overcomes the notorious aggregation-caused quenching (ACQ) effect that conventional fluorescent molecules normally suffer in their aggregated or solid state,[4] and makes the AIE-active molecules promising candidates as "turn-on" fluorescent probes,[5] sensors,[6] bioimaging agents,[7] and even key components of electronic devices.[8]

However, the biggest drawback of the nonplanar topology of AIE active molecules is their poor ability of self-assembling, so that well-defined fluorescent nanostructures based on AIE molecules are very rare among thousands of AIE molecules ever created.[5,9−12] With regard to various fluorescent nanostructures, fluorescent vesicles are most attractive because of their great potential in fabricating theranostics that display both diagnostic and therapeutic characteristics.[13−15] It is extremely difficult to directly use AIE dyes to construct vesicles, because the nonplanar structure cannot pack densely into membrane structure required for vesicle formation. To accomplish this problem, Li et al.[16] constructed a bola-form AIE molecule with two bulky hydrophobic groups covalently linked to the opposite position of the TPE core, which results in formation of the first case of vesicles with built-in fluorescence. Unfortunately, organic solvent has to be used in Li's vesicle

Received: February 12, 2018
Accepted: April 4, 2018
Published: April 4, 2018

DOI: 10.1021/acsanm.8b00226
ACS Appl. Nano Mater. 2018, 1, 1819−1827

Scheme 1. (a) Molecular Structures of TPA-1; (b) Illustration of the Self-Assembly of TPA-1/Zn^{2+} Fluorescent Vesicle Which Is Capable of Drug Loading and Displays Two-Photon Excited Emission

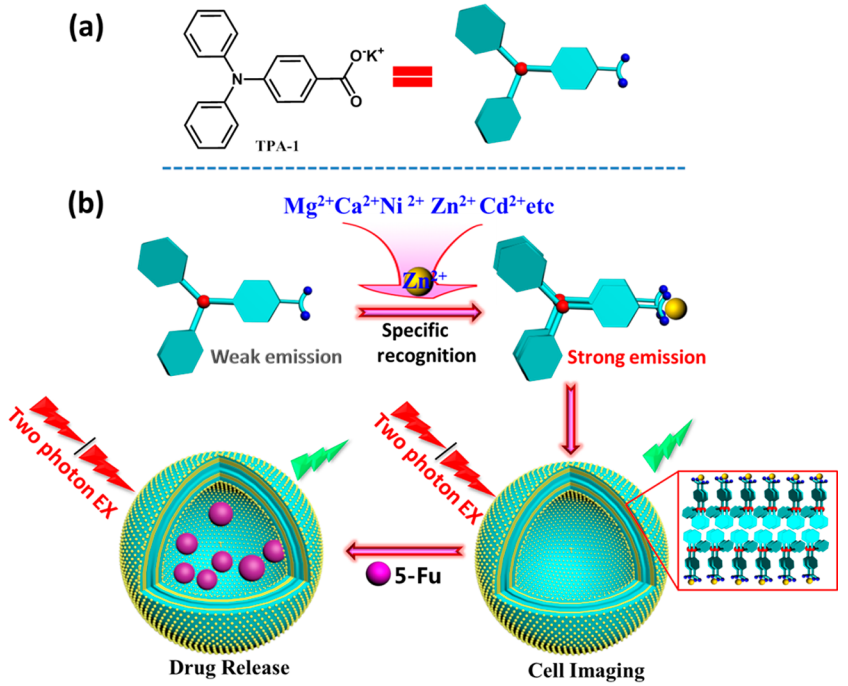

Scheme 2. Synthesis Procedure of TPA-1

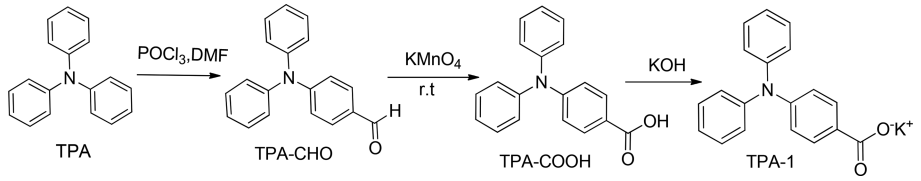

due to the poor water solubility aroused by the bulky hydrophobic group. It is highly desired to develop fluorescent vesicles in aqueous media for biological applications.

In our previous work, we proposed a straightforward ionic supra-amphiphilic method for production of fluorescent vesicles in aqueous media based on a propeller-shaped multiarmed AIE dye.[17,18] The voids between every two leaflets of the propellers can be efficiently filled by the hydrocarbon chain of the oppositely charged ionic amphiphiles, so that the supramolecular ionic complex can self-assemble into vesicles via enhanced hydrophobic effect. In an alternative design of Sessler et al.,[19] hydrophilic heads were endowed to a bola-type hydrophobic AIE dye via host−guest interaction, which results in water-soluble fluorescent vesicles. Nevertheless, the strategy of construction of supra-amphiphiles bypasses the difficulty in synthesis of water-soluble amphiphilic AIE molecules, and opens up a broad avenue toward AIE-based theronostic nanocarriers. However, so far, successful construction of fluorescent vesicles based on AIE fluorogens is still very rare.

In this work, we report the unprecedented metallo-organic vesicles based on the AIE active molecule potassium triphenylamine carboxylate (Scheme 1a). Triphenylamine (TPA) is an important structural motif in generating turn-on fluorescence for biological applications, such as biosensors and cell imaging.[20,21] This molecule takes triangular cone conformation with the N atom being the summit of the cone. The three C−N single bonds are freely rotatable which dissipates the absorbed energy just like other propeller-shaped AIE motif.[1] The fluorescence of the TPA motif can be facilely turned on through covalent or noncovalent functionalization which is sufficient to block the intramolecular rotation of phenyl rings.[22,23] In contrast to the tedious organic modification, we show that the simple TPA derivative of potassium triphenylamine carboxylate can be specifically triggered by zinc ions to form unprecedented robust metallo-organic fluorescent vesicles (Scheme 1b). The vesicle is resistant to collapse on drying, and displays two-photon emission ability. Elemental analysis and mass spectrum study reveal that the vesicle membrane is composed of the metallo-organic complex of $Zn(TPA\text{-}1)_2$. Drug-loading experiments suggest that a high loading capacity up to 53.4% can be achieved for the model anticancer drug 5-fluorouracil (5-Fu), and a gradual release of the drug is possible within 3 h. The vesicles loaded with drugs can be facilely taken up by cells via endocytosis, and the two-photon emission can be used to track the cell living status. Interestingly, the strong fluorescent vesicle can only be triggered by Zn^{2+}. The specific interaction with Zn^{2+} is not interfered by other metal ions, and the considerable fluorescent enhancement of TPA-1 is still detectable even at concentrations of Zn^{2+} down to several uM. Therefore, the present metallo-organic vesicles of 2TPA-1@Zn^{2+} is a multifunctional platform of cell imaging, drug loading, delivery tracking, and as well as a "turn-on" sensor for specific and quantitative detection of Zn^{2+}.

DOI: 10.1021/acsanm.8b00226
ACS Appl. Nano Mater. 2018, 1, 1819−1827

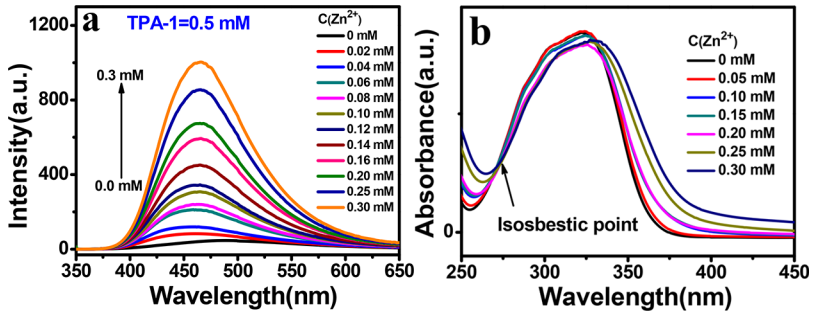

Figure 1. (a) Fluorescence spectra of 0.5 mM TPA-1 upon addition of Zn^{2+} at various concentrations (0−0.3 mM). (b) UV spectra of 0.5 mM TPA-1 with varied Zn^{2+} concentrations (0−0.3 mM). The pH remained at 7.4 for all the measurements.

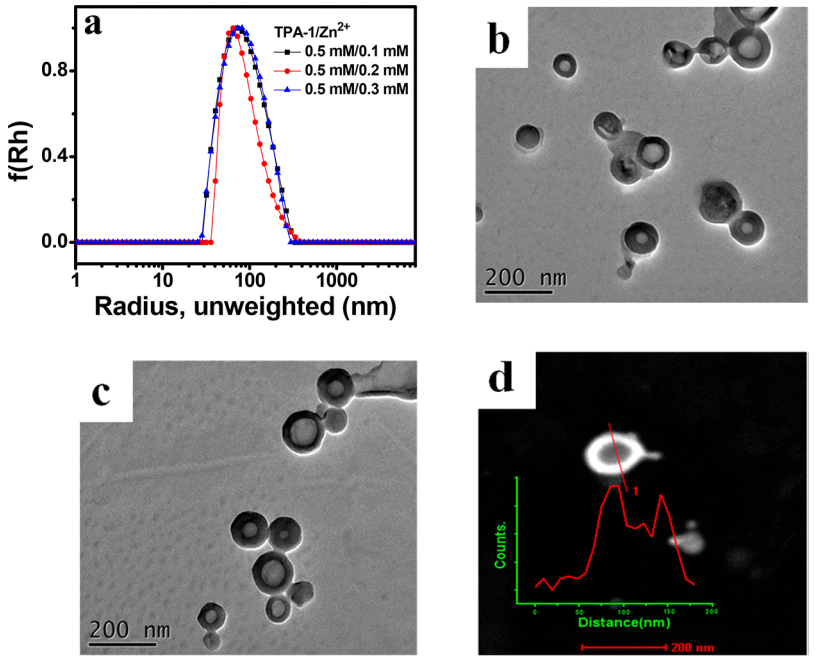

Figure 2. (a) DLS size distribution of the vesicles formed in the TPA-1/Zn^{2+} systems with varying the molar ratio between TPA-1 and Zn^{2+}. The concentration of Zn^{2+} changes from 0.1 mM to 0.3 mM at a fixed concentration of 0.5 mM TPA-1. (b, c) TEM images of the vesicles formed in the TPA-1/Zn^{2+} systems of (b) 0.5/0.1 mM and (c) 0.5/0.3 mM. (d) HAADF-STEM image of a TPA-1/Zn^{2+} vesicle. The inset is HAADF-STEM-EDS linear scan profile for the element Zn^{2+} in the vesicles in d. pH is set at 7.4 for all the systems.

2. RESULTS AND DISCUSSION

Potassium 4-carboxytriphenylamine (TPA-1) (Scheme 2) was synthesized according to literature method.[24] The pK_a of the acid form of the 4-carboxytriphenylamine is 7.1, and TPA-1 can form a transparent solution in water at pH >7.1. No Tyndall effect could be observed for solutions below 1.0 mM. These dilute solutions give very weak fluorescence with a broad peak centered at 495 nm (Figure 1a). However, upon addition of the aqueous solution of $Zn(NO_3)_2$, significant fluorescence enhancement was observed, which is accompanied by the occurrence of strong Tyndall phenomenon. This means addition of Zn^{2+} has triggered aggregation of the TPA-1 molecule. Fluorescence measurements reveal that the emission is blue-shifted to 460 nm (Figure 1a), and the quantum yield of TPA-1 is enhanced 18 folds (from Φ_{free} = 0.0147 to $\Phi_{Zn^{2+}}$ = 0.266). Compared to the UV−vis absorbance of TPA-1 peaked at 323 nm, the addition of Zn^{2+} triggers a red-shift of the absorbance to 335 nm (Figure 1b). The mirror relation of the shift in the fluorescence and in the UV−vis absorption indicate that binding of Zn^{2+} has changed the energy level of TPA-1 and the light adsorbed by the TPA-1/Zn^{2+} system is relaxed completely in the form of photon. In line with this, an isosbestic point occurs at 273 nm in the UV−vis spectra with increasing the amount of Zn^{2+} in the system, confirming the formation of a new species different from TPA-1. Meanwhile, the absorbance at wavelengths beyond 350 nm does not fall back to the baseline (Figure 1b), indicating the newly formed species have triggered the formation of colloidal particles which scatter light strongly. This is in perfect agreement with the observation of Tyndall phenomenon and increased turbidity (Figure S1) in the samples.

DLS measurements suggest the colloidal particles have an average hydrodynamic radius (R_h) around 70 nm (Figure 2a). TEM observation discloses the formation of hollow spherical particles in the 0.5 mM TPA-1 system as the concentration of Zn^{2+} is varied between 0.1−0.3 mM, indicating these structures are vesicles, which are stable over 1 week. Lower concentration of Zn^{2+} makes it difficult to find vesicles under TEM, but DLS measurements reveal there are still particles of the same size (Figure S2a). It is possible that the number of the vesicles is reduced at lower Zn^{2+} concentration. However, further increase the concentration of Zn^{2+}, for instance, to 0.4 mM, causes

DOI: 10.1021/acsanm.8b00226
ACS Appl. Nano Mater. 2018, 1, 1819−1827

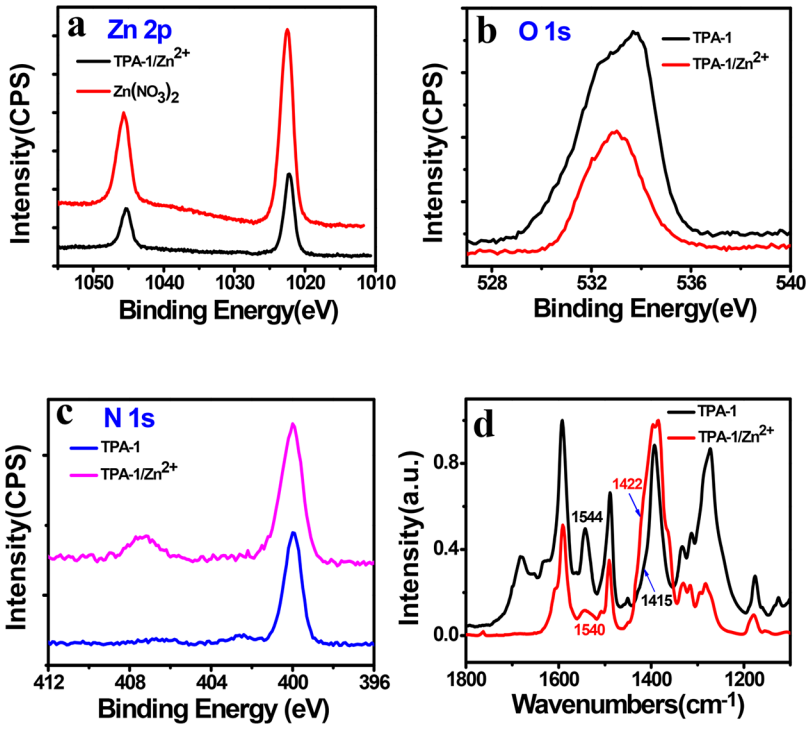

Figure 3. (a–c) The XPS measurement of the binding energy of electrons for (a) Zn 2p, (b O 1s), and N 1s orbitals, respectively, in the TPA-1/Zn^{2+} system. Corresponding control experiments made with the single system of Zn^{2+} and TPA-1 are provided for each measurements. All the samples in a–c are deposited on silicon substrates. (d) FT-IR spectra of the TPA-1 (black) and TPA-1/Zn^{2+} (red). TPA-1/Zn^{2+} = 0.5/0.3 mM for all the measurements.

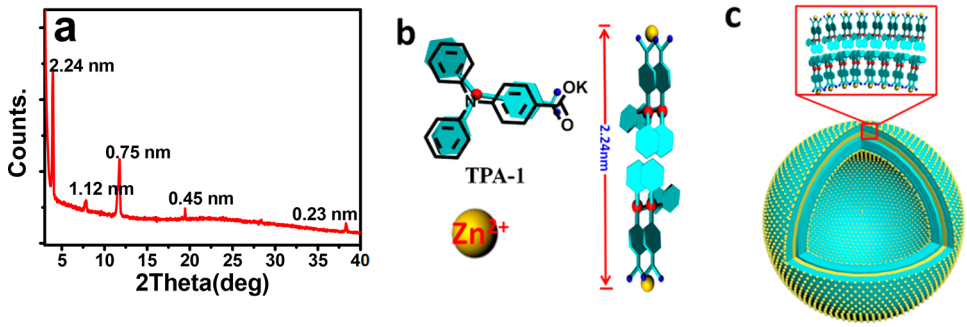

Figure 4. (a) PXRD patterns of the TPA-1/Zn^{2+} system on glass sheet, (b) illustration of the formation of bilayer structure with TPA-1 and Zn^{2+} that further stacks into vesicle membrane, and (c) illustration of the structure of a multilamellar vesicle.

precipitates. SEM observation reveals the occurrence of cross-linking of the vesicles (Figure S2b). Therefore, in the following study, the Zn^{2+} concentration of 0.3 mM is used to fabricate vesicles because this is optimal condition to obtained stable and populated vesicles. Notice that all these vesicles have walls with exclusively high electron contrast without any staining, so that the thickness of the walls can be directly read from the TEM images to be about 20 nm (Figure 2b, c and Figure S3a, b). It is noticed that both the wall thickness and the size of the vesicles are similar under different Zn^{2+} concentrations, suggesting that vesicles can only be formed by the TPA-1/Zn^{2+} complex. High angle annular dark field scanning electron microscope (HAADF-STEM) measurement reveals that the zinc element is rich in the vesicular wall (Figure 2d), which explains the extremely high contrast of the vesicle wall under TEM.

The presence of Zn^{2+} in the vesicle wall indicates that the vesicles are self-assembled from the metallo-organic complex formed by TPA-1 and Zn^{2+}. To get more insight about the interaction between TPA-1 and Zn^{2+}, X-ray photoelectron spectroscopy (XPS) measurements were performed. Figure 3a shows that the binding energy for Zn 2p electrons is decreased by 0.5 eV and that for the O 2p electrons is increased by 0.9 eV (Figure 3b), whereas no obvious binding energy shift appear in the N 2p electrons (Figure 3c). These data verify that the zinc ion is bound to the oxygen of the carboxylate group in TPA-1. However, FT-IR measurements (Figure 3d) reveal that the asymmetric (1540 cm^{-1}) and symmetric (1422 cm^{-1}) stretching vibration of C═O does not change significantly, but the relative intensity of the two peak changes drastically, suggesting Zn^{2+} has electrostatically interacted with the $-COO^-$ group. This means there should be the charge neutral 2TPA-1@Zn^{2+} building block in the vesicles. Such a scenario is further confirmed with energy-dispersive X-ray spectroscopy (EDX) and mass spectrometry analysis. EDX measurement (Figure S4) demonstrates that the molar ratio between TPA-1 and Zn^{2+} is close to 2:1, whereas a peak at m/z = 679.63,

DOI: 10.1021/acsanm.8b00226
ACS Appl. Nano Mater. 2018, 1, 1819–1827

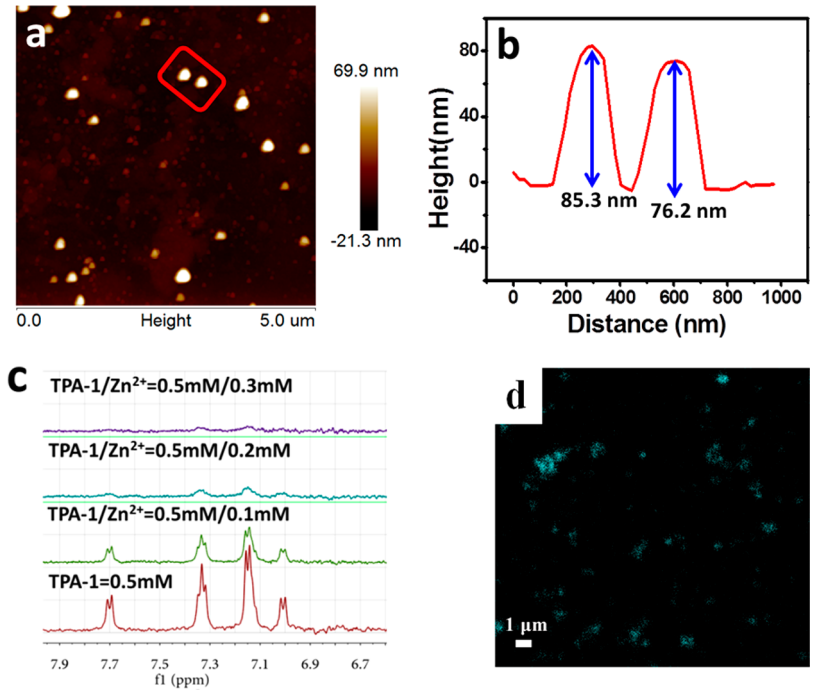

Figure 5. (a) AFM image of the vesicles formed in the TPA-1/Zn^{2+} (0.5 mM/0.3 mM) system. (b) Height profile of the circled vesicle membrane in a. (c) ^{1}H NMR spectra of the 0.5 mM TPA-1 with addition of 0.0−0.3 mM Zn^{2+}. (d) CLSM image for the vesicles formed in the TPA-1/Zn^{2+} system at pH 7.4 excited under 405 nm laser.

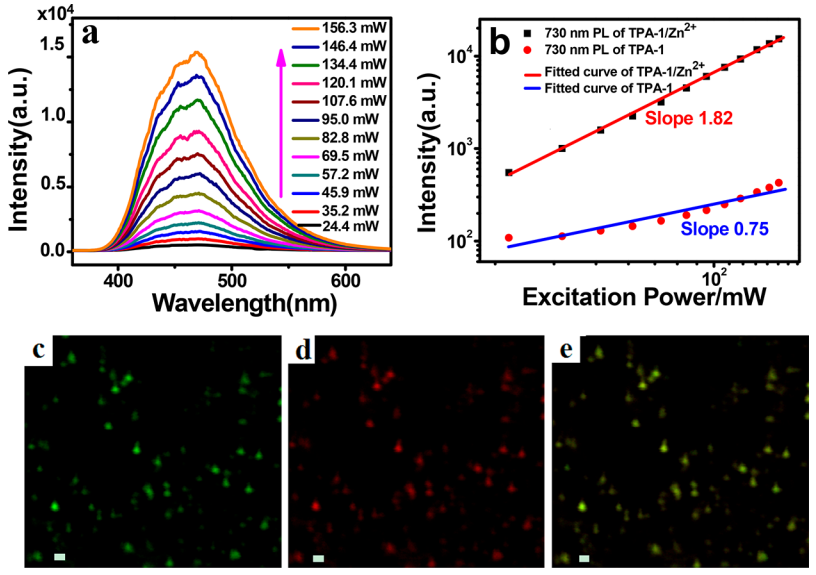

Figure 6. Two-photon emission properties of the 0.5 m TPA-1/0.3 mM $Zn(NO_3)_2$ system.(a) The upconversion PL spectra obtained at various excitation intensities, λex: 730 nm; (b) The linear relationship between the PL intensity and excitation power (mW); (c)-(e) Fluorescence image of the vesicles observed under two-photon excitation mode. (c) Image collected in the range of 420−475 nm; (d) image collected in the range of 500−550 nm; (e) the overlap of c and d, λ_{ex}: 800 nm. Scale bar: 1 μm.

corresponding to $[(2TPA\text{-}1@Zn^{2+})K]^+$, is clearly observed in the Mass spectrometry (see Figure S5) for the $Zn(TPA\text{-}1)_2$ complexes. It is noteworthy that the 2:1 complex is observed for the TPA-1/Zn^{2+} systems prepared at different starting ratios (see Figures S6 and S7), conforming that the vesicles are formed by the charge neutral complex of 2TPA-1@Zn^{2+}. It is possible that the neutral 2TPA-1@Zn^{2+} has enhanced hydrophobic effect compared to the charged TPA-1 monomer, so that vesicle formation becomes possible in the 2TPA-1@Zn^{2+} system.

Powder X-ray diffraction (PXRD) measurements of TPA-1/Zn^{2+} provide insights about the molecular arrangement in the vesicle membrane. The PXRD pattern (Figure 4a) of 2TPA-1@Zn^{2+} vesicles shows a set of peaks corresponding to the *d*-spacing of 2.24 nm, 1.12 nm, 0.75 nm, 0.45 and 0.23 nm, featuring the 001, 002, 003, 005, 0010 diffractions of a perfect lamellar structure. The distance corresponding to the intense 001 diffraction is 2.24 nm, which is two times of the length of the $Zn(TPA\text{-}1)_2$ molecule. This means the tail-to-tail arranged bilayer of $Zn(TPA\text{-}1)_2$, as illustrated in Figure 4b, is the basic

DOI: 10.1021/acsanm.8b00226
ACS Appl. Nano Mater. 2018, 1, 1819−1827

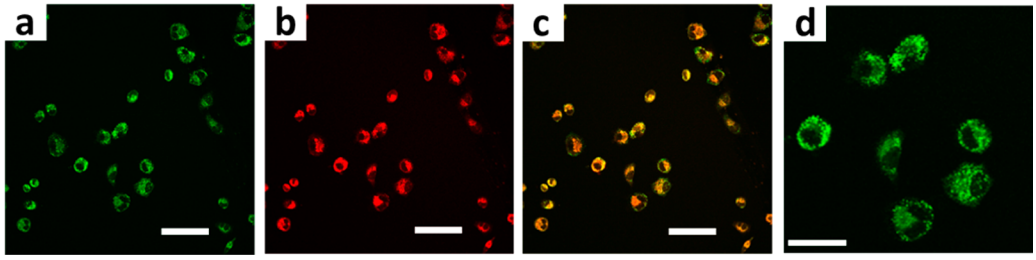

Figure 7. Two-photon Hela cell image following a 12 h treatment with TPA-1/Zn^{2+} (50 μM, 2:1 ratio). (a) Emission wavelength from 420 to 475 nm. (b) Emission wavelength from 500 to 550 nm. (c) Overlay of a and b. Scale bar: 100 μm. (d) Enlarged image from a. Scale bar: 50 μm. λ_{ex}: 800 nm.

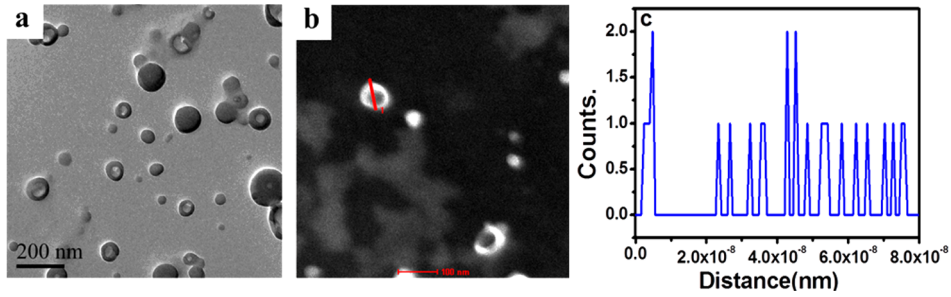

Figure 8. (a) TEM images of TPA-1/Zn^{2+} (0.5 mM/0.3 mM) vesicles loaded with 5-Fu; (b)HAADF-STEM image of TPA-1/Zn^{2+} vesicles loaded with 5-Fu; (c) HAADF-STEM-EDS linear scan profile for the element F in 5-Fu in the vesicles in b. pH is set at 7.4 for all the systems.

structural unit of the vesicle membrane. However, we believe there should be some extra TPA-1 molecules coassemble with the $Zn(TPA\text{-}1)_2$ complex to form vesicles, because the zeta potential for the vesicles is in the range of −41 to −33 mV (Table S1). Recalling the 20 nm membrane thickness, we are confident that the vesicles are predominantly multilamellar, as illustrated in Figure 4c.

The metallo-organic vesicles formed by $Zn(TPA\text{-}1)_2$ complex is very robust. AFM measurements (Figure 5a) indicate that the height of the dried vesicles can be 85.3 nm (Figure 5b), which is very close to the diameter of the vesicles obtained in TEM and DLS measurements, suggesting the vesicles are very stiff so that they do not collapse upon drying. This is further verified by ^{1}H NMR measurements. Figure 5c shows that upon addition of Zn^{2+} to the aqueous solution of TPA-1, the signal for the protons on the benzene ring vanish gradually, indicating the TPA-1 molecules assembled very tightly in the vesicle membrane. CLSM observation reveals that these metallo-organic vesicles display strong fluorescence (Figure 5d), suggesting the origin of the fluorescence enhancement of TPA-1 is the formation of fluorescent vesicles.

Interestingly, as the excitation wavelength is doubled, the fluorescence from 2TPA@Zn^{2+} vesicles is observed as well (Figure 6a). In line with this, the slope of the linear excitation power−emission intensity plot is nearly 2 (Figure 6b), indicating the metallo-organic vesicles are capable of two-photon emission. The two photon absorption cross-section of TPA-1/Zn^{2+} is about 7.3 GM (1 GM = 1×10^{-50} cm^4 s per photon, λ_{ex}: 730 nm), which is applicable for imaging.[25] In contrast, two-photon process for the single TPA-1 system is not possible, as is revealed by the slope of 1 in Figure 6b. Figure 6c−e demonstrate the vesicles observed under two-photo emission mode. As the excitation is set at 800 nm, fluorescent particles can be observed both in the channel of 420−475 nm (Figure 6c) and 500−550 nm (Figure 6d), which are within the emission range of TPA-1.

Next, the two-photon emitting vesicles were tested for cell imaging. HaLa cells were incubated in solution containing the vesicle of 2TPA-1@ Zn^{2+} for 12 h, and two photon microscopy images were then obtained by exciting the probes with a mode-locked titanium−sapphire laser source set at wavelength 800 nm. Green and red emissions were clearly observed in the channel of 420−475 nm and 500−550 nm (Figure 7a−c), confirming the excellent two-photon imaging ability of the metallo-organic vesicles in Figure 6. Note that Figure 7c reveals that the color Figure 7A is not fully overlap with 7B. The possible reason is the wavelength dependent scattering of light by organelle in cells. Enlarged CLSM image indicates the fluorescence is homogeneously distributed in the cytosol (Figure 7d). It is possible that some organelle specifically scatters the green or the red component of the emission. Nevertheless, it is very amazing that the negatively charged vesicles have entered HaLa cells without any difficulty, since one would expect the negatively charged membrane of HaLa cells would repel the cocharged vesicles. We assume the zinc ions on the surface of the vesicles may help to coordinate to the carboxylate groups on the cell surface, which facilitates endocytosis process.

Drug loading tests of the vesicles was made using the model drug 5-Fluorouracil (5-Fu), a small water-soluble antimetabolite compound that can prevent tumor-cell pyrimidine nucleotide synthesis. 5-Fu was added into the aqueous suspension of $Zn(NO_3)_2$, then TPA-1 was added to form vesicles. TEM observation (Figure 8a) indicates that 5-Fu does not affect the vesicular structure of 2TPA-1@Zn^{2+}, and HAADF-STEM measurement reveals the presence of F element in the interior of the vesicles (Figure 8 b,c), verifying that 5-Fu has been successfully entrapped into the vesicles.

Encapsulation efficiency measurements suggested that about 53.4% (w/w) of 5-Fu was encapsulated in the 2TPA-1@Zn^{2+} vesicles. Although this value is not the highest drug loading ability through literature reports, it is nearly comparable to the

DOI: 10.1021/acsanm.8b00226
ACS Appl. Nano Mater. 2018, 1, 1819−1827

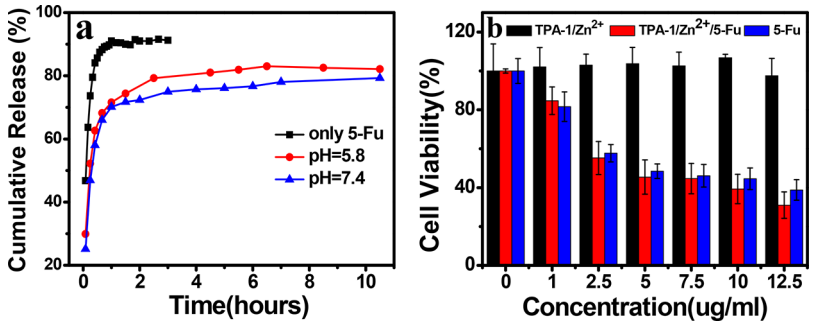

Figure 9. (a) Drug release profiles for 2TPA-1@Zn^{2+} fluorescent vesicles at pH 7.4 (blue), pH 5 (red) and only 5-Fu (black). (b) Viabilities of Hela cells in the presence of TPA-1/Zn^{2+} (A), TPA-1/Zn^{2+}/5-Fu (B). and 5-Fu (C), as assayed by MTT.

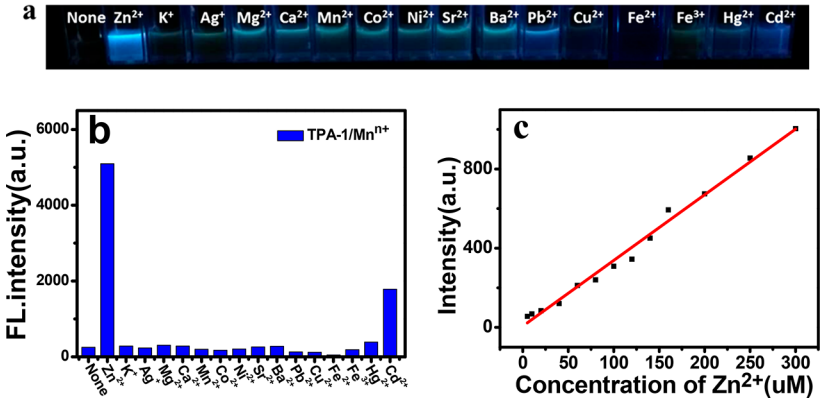

Figure 10. (a) Photos of 0.5 mM TPA-1 solution in the presence of different metal ions under irradiation of UV light (365 nm), (b) fluorescence intensity of TPA-1 (0.5 mM) with different metal ions (0.2 mM). (c) Dependence of fluorescence intensity of TPA-1 on the concentrations of Zn^{2+} at pH 7.4.

drug loading efficiency obtained in coassembly of drug with other molecules.[26] Releasing experiments (Figure 9a) reveal that the drug release from 2TPA-1@Zn^{2+} vesicles can be divided into three phases: (1) the sudden release phase within 20 min; (2) the gentle release phase within 3 h; and (3) the slow release phase last to 6 h. In practice, the sudden release of drug in the body can quickly reach an effective therapeutic concentration,[27,28] and the gentle and slow releases allow the drug in the body to remain at the effective therapeutic concentration range. This initial rapid drug release is contributed by the 5-Fu molecules adsorbed on the surface of 2TPA-1@Zn^{2+} vesicles, whereas the gentle and slow release is from the 5-Fu molecules entrapped in the interior of the 2TPA-1@Zn^{2+} vesicles. The final releasing efficiency in pH 5.8, an environment similar to cancer cells,[29] can be 83%, whereas that in the normal cell pH 7.4 environment is about 76%. Although the pH dependence is not significant, the drug releasing can still be enhanced in acidic pH, suggesting the present vesicles may be potentially used in cancer therapy.

Next, the two-photon emissive vesicle loaded with 5-Fu was used to monitor the therapeutic efficiency toward cancer cells (Figure 9b). First of all, the cytotoxicity of the unloaded vesicles was evaluated by MTT assay. After 24 h incubation with Hela cells, no obvious toxicity was observed as the concentration of $Zn(TPA\text{-}1)_2$ complex ranges from 0 to 12.5 μg/mL, indicating the good biocompatibility of the 2TPA-1@Zn^{2+} vesicles. In contrast, the cancer cell viability is significantly reduced when treated with the 2TPA-1@Zn^{2+} vesicles loaded with 5-Fu; and the cell viability is even lower than those treated only with 5-Fu, suggesting the sustained releasing of 5-Fu from the 2TPA-1@Zn^{2+} vesicles have enhanced the therapeutic effect of 5-Fu.

Finally, we found the Zn^{2+} triggered vesicle formation can also be a fluorescent platform for specific detection of Zn^{2+} in water. In recent years, fluorescent detection has attracted intensive attention because of its simplicity, high sensitivity and intracellular bioimaging capacity.[30−32] In the present study, significant fluorescence enhancement of TPA-1 was observed only for Zn^{2+}. Figure 9a shows that other metal ions, such as Fe^{2+}, Co^{2+}, Ni^{2+}, Cd^{2+}, Mg^{2+}, Sr^{2+}, Ba^{2+}, Pb^{2+}, Hg^{2+}, K^{+}, Ag^{+}, Fe^{3+}, can hardly trigger strong fluorescence of TPA-1 (Figure 10a, b), indicating the specific interaction between TPA-1 and Zn^{2+}. Note that Cd^{2+} exhibits some enhancement of the fluorescence since these two elements are in the same group of the periodic table and show similar coordination effect with many chemosensors.[33,34] Fortunately, the interference of Cd^{2+} is negligible in living cells because the level of Cd^{2+} is much lower than Zn^{2+} there.[35] Surprisingly, the specific detection of TPA-1 for Zn^{2+} is not interfered by other metal ions. Even in the presence of ions that are able to quench the fluorescence, such as Cu^{2+}, Fe^{2+}, Fe^{3+}, Pb^{2+}, and Hg^{2+}, addition of Zn^{2+} still triggers drastic fluorescence enhancement (Figure S8). We infer the high selectivity for vesicle assembly in the presence of Zn^{2+} is caused by the proper size and binding orbital of Zn^{2+}, which allows two TPA-1 molecules to form dimers, such that the dimmers can pack densely and further self-assemble into vesicles.

The fluorescence of TPA-1 displays linear dependence on the concentration of Zn^{2+} is one of the essential element in living organisms, the level of Zn^{2+} in biological systems are

DOI: 10.1021/acsanm.8b00226
ACS Appl. Nano Mater. 2018, 1, 1819−1827

much higher than the aforementioned metal ions.[36−38] The linear fluorescence titration of TPA-1 with Zn^{2+} in aqueous (Figure 10c) afforded the binding constant between TPA-1 and Zn^{2+}, $K_a = 3.9 \times 10^6\ M^{-2}$ (see the Supporting Information for calculation, Figure S9),[39,40] which is comparable to the reported excellent Zn^{2+} sensors.[41] The detection limit for Zn^{2+} is estimated as low as ~0.76 μM using the equation of $C_{DL} = 3S_b m^{-1}$ (defined by IUPAC, where S_b is the standard deviation from 10 blank solutions, and m represents the slope of the calibration curve).[42] Such a low detection limit for Zn^{2+} falls far below the normal concentration level of Zinc ion in human body (about 10 μM).[43] Therefore, we expect that TPA-1 can be used as a "turn-on" biosensor for specific detection of Zn^{2+} in biological systems.

3. CONCLUSIONS

In summary, we show in this work a case of metallo-organic fluorescent vesicle based on a simple triarylamine carboxylate AIE molecules TPA-1. Zn^{2+} ions electrostatically interact with the PTA-1 molecule to form a $Zn(TPA\text{-}1)_2$ complex, which further self-assemble into vesicles. The TPA-1 molecules are firmly confined in the vesicle membrane, thus displaying aggregation-induced emission. The condensed membrane also allows two-photon emission, which makes the vesicles excellent cell imaging agent. In combination with the ability of drug loading, the fluorescent vesicles immediately display theranostic ability. We expect that with supramolecular strategy, AIE modecules can be made into fluorescent vesicles, which opens up a new avenue for the fabrication theranostics. Furthermore, since the fluorescence is highly dependent on the electronic structure of metal ions, this strategy may simultaneously suitable for fabrication of sensors toward specific detection of metal ions. We believe that this study provides a versatile platform for cell imaging, drug carrying, and metal ion detection.

■ ASSOCIATED CONTENT

Supporting Information

The Supporting Information is available free of charge on the ACS Publications website at DOI: 10.1021/acsanm.8b00226.

Experimental section including materials, synthesis, and methods; Supplemental figures including turbidity analysis of 0.5 mM TPA-1 with varied Zn^{2+} concentrations (0−0.3 mM) at pH 7.4 (Figure S1), DLS and SEM image of TPA-1/Zn^{2+} (Figure S2), TEM images of the vesicles in the TPA-1/Zn^{2+} systems (Figure S3), zeta potential of TPA-1/Zn^{2+} mixture (Table S1), energy-dispersive X-ray (EDX) analysis of 2TPA-1@Zn^{2+} vesicles (Figure S4), ESI-MS spectra of TPA-1/Zn^{2+} mixture at different ratio (Figures S5−S7), fluorescence intensity of TPA-1 (0.5 mM) with different metal ions in the absence or presence of Zn^{2+} (Figure S9) (PDF)

■ AUTHOR INFORMATION

Corresponding Author

*E-mail: yunyan@pku.edu.cn.

ORCID

Yun Yan: 0000-0001-8759-3918

Notes

The authors declare no competing financial interest.

■ ACKNOWLEDGMENTS

Authors are grateful to National Natural Science Foundation of China (Grants 21573011 and 21422302) and the Beijing National Laboratory for Molecular Sciences (BNLMS) for financial support.

■ REFERENCES

(1) Hong, Y.; Lam, J. W.; Tang, B. Z. Aggregation-Induced Emission: Phenomenon, Mechanism and Applications. *Chem. Commun.* **2009**, 4332−4353.

(2) Hong, Y.; Lam, J. W.; Tang, B. Z. Aggregation-Induced Emission. *Chem. Soc. Rev.* **2011**, *40*, 5361−5388.

(3) Mei, J.; Hong, Y.; Lam, J. W. Y.; Qin, A.; Tang, Y.; Tang, B. Z. Aggregation - Induced Emission: The Whole Is More Brilliant than the Parts. *Adv. Mater.* **2014**, *26*, 5429−5479.

(4) Birks, J. B. *Photophysics of Aromatic Molecules*. Wiley: London, 1970; Vol. *21*, p 704.

(5) Hu, J. Y.; Liu, R.; Zhai, S. L.; Wu, Y. N.; Zhang, H. Z.; Cheng, H. T.; Zhu, H. J. AIE-Active Molecule-based Self-Assembled Nano-Fibrous Films for Sensitive Detection of Volatile Organic Amines. *J. Mater. Chem. C* **2017**, *5*, 11781−11789.

(6) Ding, D.; Li, K.; Liu, B.; Tang, B. Z. Bioprobes Based on AIE Fluorogens. *Acc. Chem. Res.* **2013**, *46*, 2441−2453.

(7) Chen, S.; Hong, Y.; Liu, Y.; Liu, J.; Leung, C. W. T.; Li, M.; Kwok, R. T. K.; Zhao, E.; Lam, J. W. Y.; Yu, Y.; Tang, B. Z. Full-Range Intracellular pH Sensing by An Aggregation-Induced Emission-Active Two-Channel Ratiometric Fluorogen. *J. Am. Chem. Soc.* **2013**, *135*, 4926−4929.

(8) Deng, J.; Xu, Y.; Liu, L.; Feng, C.; Tang, J.; Gao, Y.; Wang, Y.; Yang, B.; Lu, P.; Yang, W.; Ma, Y. An Ambipolar Organic Field-Effect Transistor Based on An AIE-Active Single Crystal with A High Mobility Level of 2.0 $cm^2\ V^{-1}\ s^{-1}$. *Chem. Commun.* **2016**, *52*, 2370−2373.

(9) Li, X.; Jiang, M.; Lam, J. W. Y.; Tang, B. Z.; Qu, J. Y. Mitochondrial Imaging with Combined Fluorescence and Stimulated Raman Scattering Microscopy Using a Probe of the Aggregation-Induced Emission Characteristic. *J. Am. Chem. Soc.* **2017**, *139*, 17022−17030.

(10) Lu, H.; Zheng, Y.; Zhao, X.; Wang, L.; Ma, S.; Han, X.; Xu, B.; Tian, W.; Gao, H. Highly Efficient Far Red/Near-Infrared Solid Fluorophores: Aggregation-Induced Emission, Intramolecular Charge Transfer, Twisted Molecular Conformation, and Bioimaging Applications. *Angew. Chem., Int. Ed.* **2016**, *55*, 155−159.

(11) Nicol, A.; Kwok, R. T. K.; Chen, C.; Zhao, W.; Chen, M.; Qu, J.; Tang, B. Z. Ultrafast Delivery of Aggregation-Induced Emission Nanoparticles and Pure Organic Phosphorescent Nanocrystals by Saponin Encapsulation. *J. Am. Chem. Soc.* **2017**, *139*, 14792−14799.

(12) Wang, J.; Gu, X.; Zhang, P.; Huang, X.; Zheng, X.; Chen, M.; Feng, H.; Kwok, R. T. K.; Lam, J. W. Y.; Tang, B. Z. Ionization and Anion-pi(+) Interaction: A New Strategy for Structural Design of Aggregation-Induced Emission Luminogens. *J. Am. Chem. Soc.* **2017**, *139*, 16974−16979.

(13) Lee, H.-K.; Park, K. M.; Jeon, Y. J.; Kim, D.; Oh, D. H.; Kim, H. S.; Park, C. K.; Kim, K. Vesicle Formed by Amphiphilc Cucurbit[6]-uril: Versatile, Noncovalent Modification of the Vesicle Surface, and Multivalent Binding of Sugar-Decorated Vesicles to Lectin. *J. Am. Chem. Soc.* **2005**, *127*, 5006−5007.

(14) Zhang, X.; Rehm, S.; Safont-Sempere, M. M.; Wurthner, F. Vesicular Perylene Dye Nanocapsules as Supramolecular Fluorescent pH Sensor Systems. *Nat. Chem.* **2009**, *1*, 623−629.

(15) Wang, X.; Yang, Y.; Zuo, Y.; Yang, F.; Shen, H.; Wu, D. Facile Creation of FRET Systems From a pH-Responsive AIE Fluorescent Vesicle. *Chem. Commun. (Cambridge, U. K.)* **2016**, *52*, 5320−3.

(16) Zhang, M.; Yin, X.; Tian, T.; Liang, Y.; Li, W.; Lan, Y.; Li, J.; Zhou, M.; Ju, Y.; Li, G. AIE-Induced Fluorescent Vesicles Containing Amphiphilic Binding Pockets and the FRET Triggered by Host−Guest Chemistry. *Chem. Commun.* **2015**, *51*, 10210−10213.

DOI: 10.1021/acsanm.8b00226
ACS Appl. Nano Mater. 2018, 1, 1819−1827

(17) Li, J.; Liu, K.; Han, Y.; Tang, B. Z.; Huang, J.; Yan, Y. Fabrication of Propeller-Shaped Supra-Amphiphile for Construction of Enzyme-Responsive Fluorescent Vesicles. *ACS Appl. Mater. Interfaces* **2016**, *8*, 27987−27995.
(18) Li, J.; Liu, K.; Chen, H.; Li, R.; Drechsler, M.; Bai, F.; Huang, J.; Tang, B. Z.; Yan, Y. Functional Built-In Template Directed Siliceous Fluorescent Supramolecular Vesicles as Diagnostics. *ACS Appl. Mater. Interfaces* **2017**, *9*, 21706−21714.
(19) Chi, X.; Zhang, H.; Vargas-Zúñiga, G. I.; Peters, G. M.; Sessler, J. L. A Dual-Responsive Bola-Type Supra-amphiphile Constructed from a Water-Soluble Calix[4]pyrrole and a Tetraphenylethene-Containing Pyridine Bis-N-oxide. *J. Am. Chem. Soc.* **2016**, *138*, 5829−5832.
(20) Xue, P.; Chen, P.; Jia, J.; Xu, Q.; Sun, J.; Yao, B.; Zhang, Z.; Lu, R. A Triphenylamine-Based Benzoxazole Derivative as A High-Contrast Piezofluorochromic Material Induced by Protonation. *Chem. Commun.* **2014**, *50*, 2569−2571.
(21) Gao, Y. T.; Qu, Y.; Jiang, T.; Zhang, H.; He, N. N.; Li, B.; Wu, J. C.; Hua, J. L. Alkyl-Triphenylamine End-Capped Triazines With AIE and Large Two-Photon Absorption Cross-Sections for Bioimaging. *J. Mater. Chem. C* **2014**, *2*, 6353−6361.
(22) Park, J.; Seo, J.; Jung, H. K.; Hyun, G.; Park, S. Y.; Jeon, S. Direct Optical Fabrication of Fluorescent, Multilevel 3D Nanostructures for Highly Efficient Chemosensing Platforms. *Adv. Funct. Mater.* **2016**, *26*, 7170−7177.
(23) Hariharan, P. S.; Mothi, E. M.; Moon, D.; Anthony, S. P. Halochromic Isoquinoline with Mechanochromic Triphenylamine: Smart Fluorescent Material for Rewritable and Self-Erasable Fluorescent Platform. *ACS Appl. Mater. Interfaces* **2016**, *8*, 33034−33042.
(24) Veronese, L.; Procopio, E. Q.; De Rossi, F.; Brown, T. M.; Mercandelli, P.; Mussini, P.; D'Alfonso, G.; Panigati, M. New Dinuclear Hydrido-Carbonyl Rhenium Complexes Designed as Photosensitizers in Dye-Sensitized Solar Cells. *New J. Chem.* **2016**, *40*, 2910−2919.
(25) Xu, C.; Zipfel, W.; Shear, J. B.; Williams, R. M.; Webb, W. W. Multiphoton Fluorescence Excitation: New Spectral Windows for Biological Nonlinear Microscopy. *Proc. Natl. Acad. Sci. U. S. A.* **1996**, *93*, 10763−10768.
(26) Gao, X.; Hai, X.; Baigude, H.; Guan, W.; Liu, Z. Fabrication of Functional Hollow Microspheres Constructed from MOF Shells: Promising Drug Delivery Systems with High Loading Capacity and Targeted Transport. *Sci. Rep.* **2016**, *6*, 37705.
(27) Tan, L. L.; Song, N.; Zhang, S. X. A.; Li, H. W.; Wang, B.; Yang, Y. W. Ca^{2+}, pH and Thermo Triple-Responsive Mechanized Zr-based MOFs for On-Command Drug Release in Bone Diseases. *J. Mater. Chem. B* **2016**, *4*, 135−140.
(28) Wang, J.; Liu, C.; Shuai, Y.; Cui, X.; Nie, L. Controlled Release of Anticancer Drug Using Graphene Oxide as A Drug-Binding Effector in Konjac Glucomannan/sodium Alginate Hydrogels. *Colloids Surf., B* **2014**, *113*, 223−229.
(29) Damaghi, M.; Wojtkowiak, J.; Gillies, R. pH Sensing and Regulation in Cancer. *Front. Physiol.* **2013**, *4*, 1−10.
(30) Xie, Y.; Wei, P.; Li, X.; Hong, T.; Zhang, K.; Furuta, H. Macrocycle Contraction and Expansion of a Dihydrosapphyrin Isomer. *J. Am. Chem. Soc.* **2013**, *135*, 19119−19122.
(31) Ding, Y.; Tang, Y.; Zhu, W.; Xie, Y. Fluorescent and Colorimetric Ion Probes Based on Conjugated Oligopyrroles. *Chem. Soc. Rev.* **2015**, *44*, 1101−1112.
(32) Ding, Y.; Zhu, W.-H.; Xie, Y. Development of Ion Chemosensors Based on Porphyrin Analogues. *Chem. Rev.* **2017**, *117*, 2203−2256.
(33) Lin, W.; Buccella, D.; Lippard, S. J. Visualization of Peroxynitrite-Induced Changes of Labile Zn^{2+} in the Endoplasmic Reticulum with Benzoresorufin-Based Fluorescent Probes. *J. Am. Chem. Soc.* **2013**, *135*, 13512−13520.
(34) Mao, Z.; Hu, L.; Dong, X.; Zhong, C.; Liu, B.-F.; Liu, Z. Highly Sensitive Quinoline-Based Two-Photon Fluorescent Probe for Monitoring Intracellular Free Zinc Ions. *Anal. Chem.* **2014**, *86*, 6548−6554.
(35) Meng, X.; Wang, S.; Li, Y.; Zhu, M.; Guo, Q. 6-Substituted Quinoline-based Ratiometric Two-photon Fluorescent Probes for Biological Zn^{2+} Detection. *Chem. Commun.* **2012**, *48*, 4196−4198.
(36) Rae, T. D.; Schmidt, P. J.; Pufahl, R. A.; Culotta, V. C.; O'Halloran, T. V. Undetectable Intracellular Free Copper: The Requirement of a Copper Chaperone for Superoxide Dismutase. *Science* **1999**, *284*, 805−808.
(37) Komatsu, K.; Urano, Y.; Kojima, H.; Nagano, T. Development of an Iminocoumarin-Based Zinc Sensor Suitable for Ratiometric Fluorescence Imaging of Neuronal Zinc. *J. Am. Chem. Soc.* **2007**, *129*, 13447−13454.
(38) Xu, Z.; Baek, K.-H.; Kim, H. N.; Cui, J.; Qian, X.; Spring, D. R.; Shin, I.; Yoon, J. Zn^{2+}-Triggered Amide Tautomerization Produces a Highly Zn^{2+}-Selective, Cell-Permeable, and Ratiometric Fluorescent Sensor. *J. Am. Chem. Soc.* **2010**, *132*, 601−610.
(39) Wei, X.; Bu, L.; Tang, W.; Zhao, S.; Xie, Y. Selective and Sensitive Fluorescence "turn-on" Zn^{2+} Probes Based on Combination of Anthracene, Diphenylamine and Dipyrrin. *Sci. China: Chem.* **2017**, *60*, 1212−1218.
(40) Bourson, J.; Pouget, J.; Valeur, B. Ion-Respnsive Fluorescent Compounds 0.4. Effect of Cation Binding On the Photophysical Properties of A Coumarin Linked to Monoaza-Crown and Diaza-Crown Ethers. *J. Phys. Chem.* **1993**, *97*, 4552−4557.
(41) Li, Y.; Li, K.; He, J. A "Turn-on" Fluorescent Chemosensor for the Detection of Zn(II) in Aqueous Solution at Neutral pH and Its Application in Live Cells Imaging. *Talanta* **2016**, *153*, 381−385.
(42) Thomsen, V.; Schatzlein, D.; Mercuro, D. Limits of Detection in Spectroscopy. *Spectrosc* **2003**, *18*, 112−114.
(43) Jiang, J.-Q.; Sun, C.-L.; Shi, Z.-F.; Xu, Z.-G.; Zhang, H.-L. A ppb Level Turn-on Fluorescence Chemosensor for the Detection of Zn^{2+}. *Sens. Actuators, B* **2015**, *220*, 659−664.

DOI: 10.1021/acsanm.8b00226
ACS Appl. Nano Mater. 2018, 1, 1819−1827